JAMECH
Vol. 45, No. 1, Sep. 2014,pp 61- 75

Large Amplitude Vibration Analysis of Graphene Sheets as Resonant Mass Sensors Using Mixed Pseudo-Spectral and Integral Quadrature Methods

S. Kamal Jalali[1*], M. Hassan Naei[2]

1. PhD Student, School of Mechanical Engineering, University of Tehran, Tehran, Iran

2. Associate Professor, School of Mechanical Engineering, University of Tehran, Tehran, Iran

Received 6 September 2014; Accepted 30 November 2014

Abstract

The present paper investigates the potential application of graphene sheets with attached nanoparticles as resonant sensors by introducing a nonlocal shear deformation plate model. To take into account an elastic connection between the nanoplate and the attached nanoparticle, the nanoparticle is considered as a mass-spring system. Then, a combination of pseudo-spectral and integral quadrature methods is implemented to numerically determine the frequency shift caused by the attached mass-spring system for both clamped and simply supported boundary conditions. The obtained results are in a good agreement with those available in the literature, which reveals that the proposed combined method provides accurate results for structural problems related to concentrated objects. The results show that for soft connections with small spring constant values, the predicted frequency shift is greater than for rigid connections. This means that considering a rigid connection instead of elastic one will underestimate the frequency shift of nano resonant sensors. Additionally, it is shown that neglecting nonlocal small scale parameter results in overestimating the frequency shift of nano resonant sensors. The presented results can be useful as a guideline for designing plane shape nano resonant sensors like graphene-based mass sensors.

Keywords: *graphene, resonant mass sensors, nonlocal elasticity, pseudo-spectral method, IQ method*

1. Introduction

In recent years, nanotechnology has found a significant role in our life due to the wide scope of its potential application in medicine, food industries, environment and energy issues and manufacturing processes, among others [1, 2]. To design future nanoscale devices, nanostructures as new members in structural mechanics have received notable attention and therefore, prediction of the response of these elements against various mechanical loading situations is important. To consider the structural discreteness of nanostructures, the nonlocal version of Eringen's continuum of elasticity [3] along with introducing small scale

* Corresponding Author. Tel.:+989197398314
Email Address: skjalali@ut.ac.ir

effects should be applied [4-7]. Reports reveal that the results obtained by nonlocal elasticity are in good agreement with those obtained by atomistic approaches.

Sensing nanoscale objects is one of the most significant issues in nanotechnology. Among various available methods for sensing applications, gigahertz nano resonant sensors, which detect these objects using vibration characteristics, have been addressed by many researchers [8]. The detection criterion is established based on measuring the resonant frequency shift of the sensor caused by the attached object due to changes in the total mass of the system. The potential of graphene sheets as nano resonant sensors has been addressed by many researchers because of their proper size, large surface area and high bending flexibility. Due to its flat shape, graphene can easily be considered as a nanoplate and related continuum theories can be adapted to analyse its frequency response.

Shen et al. [9] studied the potential of SLGSs as nano mass sensors by considering the graphene sheet as a rectangular nanoplate with concentrated attached masses based on nonlocal Kirchhoff plate theory and the Galerkin method. The effects of the mass value and position on the frequency shift were discussed. Additionally, using Kirchhoff nonlocal plate theory and the Galerkin method, Zhou et al. [10] analyzed a circular graphene sheet carrying a nanoparticle as a nano resonant mass sensor. Murmu and Adhikari [11] proposed a nonlocal mass sensor model based on vibrating monolayer cantilever graphene sheets. Closed-form equations were derived for the frequency shift due to the added mass. However, their work was limited to lined shape distribution of the masses and linear vibration analysis. Neglecting small scale effects, in a similar study, Adhikari and Chowdhury [12] investigated the possibility of implementing graphene sheets as nano resonant sensors. Lee et al. [13] mass detection using a graphene-based nano resonator in the framework of nonlocal elasticity. The graphene sheet was considered as a rectangular nanoplate with an attached mass and equations of motion were analytically solved for simply supported boundary conditions. Influence of the small scale effect and the size and aspect ratio of SLGS on the sensitivity of the sensor was discussed in detail. In order to investigate the possibility of double layered graphene sheets as resonant mass sensors, Natsoki et al. [14] studied the vibration of double-layered rectangular graphene sheet resonators as nanoplates using the local continuum elasticity theory.

Reviewing the literature, it is observed that geometric nonlinearity has a significant role in the large amplitude vibration of graphene sheets and resonant frequency is related to vibration amplitude [15-20]. However, the simultaneous influence of geometric nonlinearity and nonlocality on the frequency shift and sensitivity of nano resonant sensors has not been reported. In this study, application of SLGSs as resonant sensors in the detection of nanoparticles is investigated. Furthermore, to take into consideration the effect of nonlinearity, nonlocality and atomic interactions between SLGSs and attached nanoparticles, a nonlinear nonlocal plate model with an attached mass-spring system is introduced.

2. Nonlocal shear deformation plate model

A nonlocal continuum model for the nonlinear vibration of an SLGS with attached nanoparticles on its surface is proposed. According to its two dimensional geometry, a graphene sheet may be represented by an elastic nanoplate of length a, width b, the effective thickness h and mass density p. To take into account the contact interactions in nonlocal formulation, the attached nanoparticle is considered as a mass-spring system (M_0, K_0) mounted on an arbitrary position (x_0,y_0) of the plate. The coordinate system (x,y,z) is located at the corner of the plate, such that the plate mid-plane coincides with xy plane and the z-axis is normal to it, as illustrated in Figure 1. Invoking Von Kármán's large deflection assumption and the first-order shear deformation plate theory (FSDT), nonlinear strain-displacement relations can be described as [21]:

$$\varepsilon_x = \varepsilon_{x0} + zk_x \tag{1a}$$

$$\varepsilon_y = \varepsilon_{y0} + zk_y \tag{1b}$$

$$\gamma_{xy} = \gamma_{xy0} + zk_{xy} \tag{1c}$$

$$\gamma_{xz} = \gamma_{xz0} \tag{1d}$$

$$\gamma_{zy} = \gamma_{zy0} \tag{1e}$$

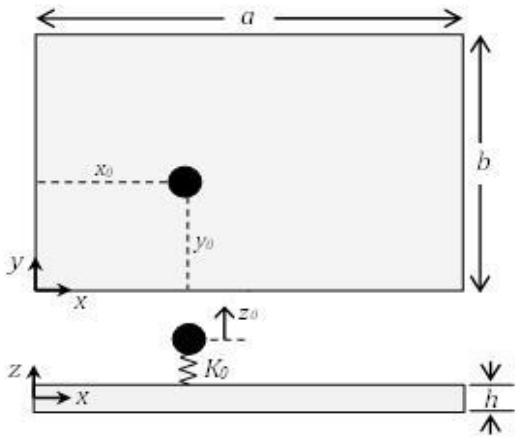

Fig. 1. Schematic of the studied nanoplate with an attached mass-spring system

The mid plane strains and curvatures are described by:

$$\varepsilon_{x0} = u_{0,x} + \frac{1}{2}(w_{0,x})^2 \ , \ k_x = \varphi_{x,x} \tag{2a}$$

$$\varepsilon_{y0} = \nu_{0,y} + \frac{1}{2}(w_{0,y})^2 \ , \ k_y = \varphi_{y,y} \tag{2b}$$

$$\gamma_{xy0} = u_{0,y} + v_{0,x} + w_{0,x}w_{0,y} \ , \ k_{xy} = \varphi_{x,y} + \varphi_{y,x} \tag{2c}$$

$$\gamma_{xz0} = \varphi_x + w_{0,x} \tag{2d}$$

$$\gamma_{zy0} = \varphi_y + w_{0,y} \tag{2e}$$

where $()_{,x}$ and $()_{,y}$ indicate the differentiation with respect to *x* and *y*, respectively. Additionally, u_0, v_0 and w_0 are the mid-plane displacement components along the *x*, *y* and *z* directions, while φ_x and φ_y define rotation about the *y* and *x* axis, respectively.

Nonlocal continuum elasticity assumptions appear in constitutive stress-strain relations. In conventional local elasticity, stress at a point depends only on the strain at that point. Then, the macroscopic local stress component t_{ij} at a point is related to the strain tensor component ε_{mn} at that point by generalized Hooke's law as follows:

$$t_{ij} = C_{ijmn}\varepsilon_{mn} \tag{3}$$

where C_{ijmn} is the fourth-order elasticity tensor component [21]. On the other hand, based on nonlocal elasticity assumptions first proposed by Eringen [3], the stress at a point is related to the strain at every point of the elastic body through an integration on the whole elastic body domain. Eringen [22] explained that it is then possible to represent the integral constitutive relation in an equivalent and simpler differential form as follows:

$$\left(1-\mu\nabla^2\right)\sigma_{ij} = t_{ij} = C_{ijmn}\varepsilon_{mn} \ , \ \mu = \left(e_0 a_0\right)^2 \tag{4}$$

in which $\boldsymbol{\mu}$ is the nonlocal parameter presenting the small scale effects, e_0 is a material constant, a_0 is the internal characteristic length (e.g., distance between constitutive atoms, which is C-C bond length for graphene), ∇^2 is the two-dimensional Laplace operator and σ_{ij} is the nonlocal stress component. Small scale parameter can be obtained by using atomic lattice dynamics or by comparing molecular dynamics (MD) results with nonlocal continuum models for calibrating a proper small scale parameter [7]. Setting the internal characteristic length equal to zero results in $\mu = \mathbf{0}$ reducing to the perfect continuous state of local elasticity. The nonlocal stress-strain relationship for the plane stress state of nanoplates can be written as:

$$\begin{Bmatrix} \sigma_x \\ \sigma_y \\ \tau_{zy} \\ \tau_{xz} \\ \tau_{xy} \end{Bmatrix} - \mu\nabla^2 \begin{Bmatrix} \sigma_x \\ \sigma_y \\ \tau_{zy} \\ \tau_{xz} \\ \tau_{xy} \end{Bmatrix} = \begin{bmatrix} Q & \nu Q & 0 & 0 & 0 \\ \nu Q & Q & 0 & 0 & 0 \\ 0 & 0 & G & 0 & 0 \\ 0 & 0 & 0 & G & 0 \\ 0 & 0 & 0 & 0 & G \end{bmatrix} \begin{Bmatrix} \varepsilon_x \\ \varepsilon_y \\ \gamma_{zy} \\ \gamma_{xz} \\ \gamma_{xy} \end{Bmatrix} \tag{5}$$

$$Q = \frac{E}{\left(1-\nu^2\right)'} \ , G = \frac{E}{2(1+\nu)}$$

E, *v* and *G* are Young's modulus, shear modulus and Poison's ratio of the nanoplates, respectively. One can calculate the nonlocal force and moment resultants by integrating stress components across the plate thickness.

$$\left[N_{xx}, N_{yy}, N_{xy}\right] = \int_{-h/2}^{h/2}\left[\sigma_{xx}, \sigma_{yy}, \sigma_{xy}\right]dz \tag{6a}$$

$$\left[M_{xx}, M_{yy}, M_{xy}\right] = \int_{-h/2}^{h/2}\left[\sigma_{xx}, \sigma_{yy}, \sigma_{xy}\right]z\,dz \tag{6b}$$

$$\left[Q_x, Q_y\right] = K_s\int_{-h/2}^{h/2}\left[\tau_{xz}, \tau_{zy}\right]dz \tag{6c}$$

K_s is the shear correction coefficient of FSDT, which is considered equal to 5/6 [23]. Combining Equation (5) and Equation (6), these force and moment resultants can be

expressed in terms of displacement components:

$$\begin{Bmatrix} N_{xx} \\ N_{yy} \\ N_{xy} \end{Bmatrix} - \mu\nabla^2 \begin{Bmatrix} N_{xx} \\ N_{yy} \\ N_{xy} \end{Bmatrix} = \begin{bmatrix} A & \nu A & 0 \\ \nu A & A & 0 \\ 0 & 0 & \dfrac{A(1-\nu)}{2} \end{bmatrix} \begin{Bmatrix} \varepsilon_{x0} \\ \varepsilon_{y0} \\ \gamma_{xy0} \end{Bmatrix} \quad (7a)$$

$$A = \frac{Eh}{(1-\nu^2)}$$

$$\begin{Bmatrix} M_{xx} \\ M_{yy} \\ M_{xy} \end{Bmatrix} - \mu\nabla^2 \begin{Bmatrix} M_{xx} \\ M_{yy} \\ M_{xy} \end{Bmatrix} = \begin{bmatrix} D & \nu D & 0 \\ \nu D & D & 0 \\ 0 & 0 & \dfrac{D(1-\nu)}{2} \end{bmatrix} \begin{Bmatrix} k_x \\ k_y \\ k_{xy} \end{Bmatrix} \quad (7b)$$

$$D = \frac{Eh^3}{12(1-\nu^2)}$$

$$\begin{Bmatrix} Q_x \\ Q_y \end{Bmatrix} - \mu\nabla^2 \begin{Bmatrix} Q_x \\ Q_y \end{Bmatrix} = K_s \begin{bmatrix} \dfrac{A(1-\nu)}{2} & 0 \\ 0 & \dfrac{A(1-\nu)}{2} \end{bmatrix} \begin{Bmatrix} \gamma_{xz} \\ \gamma_{zy} \end{Bmatrix} \quad (7c)$$

$$D = \frac{Eh^3}{12(1-\nu^2)}$$

The six governing equations of motion for free vibration of a shear deformable plate carrying a mass-spring system can be obtained using the principle of minimum total potential energy [23] as follows:

$$N_{xx,x} + N_{xy,y} = I_0 \ddot{u}_0 \quad (8a)$$

$$N_{yy,y} + N_{xy,x} = I_0 \ddot{v}_0 \quad (8b)$$

$$Q_{x,x} + Q_{y,y} + N(w_0) + K_0\left[z_0 - w_0(x_0, y_0)\right] \quad (8c)$$
$$\delta(x - x_0)\delta(y - y_0) = I_0 \ddot{w}_0$$

$$M_{xx,x} + M_{xy,y} - Q_x = I_2 \ddot{\varphi}_x \quad (8d)$$

$$M_{yy,y} + M_{xy,x} - Q_y = I_2 \ddot{\varphi}_y \quad (8e)$$

$$K_0\left[w_0(x_0, y_0) - z_0\right] = M_0 \ddot{z}_0 \quad (8f)$$

$(\dot{\ })$ operator denotes differentiation with respect to time, t and mass moments of inertia, I_0 and I_2 are calculated by:

$$(I_0, I_2) = \int_{-h/2}^{h/2} p(1, z^2)\, dz \quad (8g)$$

The nonlinear term $\mathcal{N}(w_0)$ in Equation (8c), can be written as follows [24]:

$$N(w_0) = N_{xx} w_{0,xx} + 2N_{xy} w_{0,xy} + N_{yy} w_{0,yy} \quad (8h)$$

Additionally, the Dirac Delta function, given in Equation (8c), is defined as:

$$\delta(x - x_0) = 0 \quad , \quad x \neq x_0$$

$$\delta(x - x_0) = \infty \quad , \quad x = x_0 \quad (8i)$$

$$\int_0^\infty f(x)\delta(x - x_0)dx = \int_0^a f(x)\delta(x - x_0)dx$$
$$= f(x_0) \quad , \; x_0 \prec a$$

Using Equation (7), one can rewrite Equation (8a-e) in terms of the displacement components.

$$A\left[\left(u_{0,xx} + w_{0,x}w_{0,xx}\right) + \nu\left(v_{0,xy} + w_{0,y}w_{0,xy}\right) + \frac{(1-\nu)}{2}\left(u_{0,yy} + v_{0,xy} + w_{0,y}w_{0,xy} + w_{0,x}w_{0,yy}\right)\right] \quad (9a)$$
$$= I_0\left(\ddot{u}_0 - \mu\ddot{u}_{0,xx} - \mu\ddot{u}_{0,yy}\right)$$

$$A\left[\nu\left(u_{0,xy} + w_{0,x}w_{0,xy}\right) + \left(v_{0,yy} + w_{0,y}w_{0,yy}\right) + \frac{(1-\nu)}{2}\left(v_{0,xx} + u_{0,xy} + w_{0,x}w_{0,xy} + w_{0,y}w_{0,xx}\right)\right] \quad (9b)$$
$$= I_0\left(\ddot{v}_0 - \mu\ddot{v}_{0,xx} - \mu\ddot{v}_{0,yy}\right)$$

$$A\left[K_s\frac{(1-\nu)}{2}\left(w_{0,xx} + w_{0,yy} + \varphi_{x,x} + \varphi_{y,y}\right) + w_{0,xx}\left[\left(u_{0,x} + \frac{1}{2}w_{0,x}^2\right) + \nu\left(v_{0,y} + \frac{1}{2}w_{0,y}^2\right)\right]\right.$$
$$\left. + w_{0,yy}\left[\left(v_{0,y} + \frac{1}{2}w_{0,y}^2\right) + \nu\left(u_{0,x} + \frac{1}{2}w_{0,x}^2\right)\right] + (1-\nu)w_{0,xy}\left(u_{0,y} + v_{0,x} + w_{0,x}w_{0,y}\right)\right] \quad (9c)$$
$$+ K_0\left[z_0 - w_0(x_0, y_0)\right]\delta(x - x_0)\delta(y - y_0) = I_0\left(\ddot{w}_0 - \mu\ddot{w}_{0,xx} - \mu\ddot{w}_{0,yy}\right)$$

$$D\left[\varphi_{x,xx} + \nu\varphi_{y,xy} + \frac{1-\nu}{2}\left(\varphi_{x,yy} + \varphi_{y,xy}\right)\right] - K_s A\frac{(1-\nu)}{2}\left(\varphi_x + w_{0,x}\right) = I_2\left(\ddot{\varphi}_x - \mu\ddot{\varphi}_{x,xx} - \mu\ddot{\varphi}_{x,yy}\right) \quad (9d)$$

$$D\left[\varphi_{y,yy}+\nu\varphi_{x,xy}+\frac{1-\nu}{2}\left(\varphi_{y,xx}+\varphi_{x,xy}\right)\right]-K_sA\frac{(1-\nu)}{2}\left(\varphi_y+w_{0,y}\right)=I_2\left(\ddot{\varphi}_y-\mu\ddot{\varphi}_{y,xx}-\mu\ddot{\varphi}_{y,yy}\right) \tag{9e}$$

$$K_0\left[w_0(x_0,y_0)-z_0\right]=M_0\ddot{z}_0 \tag{9f}$$

Equation (9c) is singular at the point (x_0, y_0), where the mass-spring system is located. However, considering Equation (8i), one can integrate Equation (9c) on the plate domain as follows:

$$\begin{aligned}\int_0^a\int_0^b\Bigg\{A\Bigg[&K_s\frac{(1-\nu)}{2}\left(w_{0,xx}+w_{0,yy}+\varphi_{x,x}+\varphi_{y,y}\right)+w_{0,xx}\left[\left(u_{0,x}+\frac{1}{2}w_{0,x}^2\right)+\nu\left(v_{0,y}+\frac{1}{2}w_{0,y}^2\right)\right]\\&+w_{0,yy}\left[\left(v_{0,y}+\frac{1}{2}w_{0,y}^2\right)+\nu\left(u_{0,x}+\frac{1}{2}w_{0,x}^2\right)\right]+(1-\nu)w_{0,xy}\left(u_{0,y}+v_{0,x}+w_{0,x}w_{0,y}\right)\Bigg]\\&-I_0\left(\ddot{w}_0-\mu\ddot{w}_{0,xx}-\mu\ddot{w}_{0,yy}\right)\Bigg\}dxdy=K_0\left[w_0(x_0,y_0)-z_0\right]\end{aligned} \tag{9g}$$

This integral form will be used in the following section for the solution procedure. Both clamped and simply supported boundary conditions can be considered in transverse direction, while in-plane boundary conditions are assumed to be fully immovable.

Clamped(CCCC):

$$At\ x=0,a\ and\ y=0,b:\ \ u_0=0,v_0=0,w_0=0,\ \varphi_x=0,\ \varphi_y=0 \tag{10a}$$

SimplySupported (SSSS):

$$\begin{aligned}&At\ x=0,a:\ \ u_0=0,v_0=0,w_0=0,\ \varphi_y=0,\ \varphi_{x,x}=0\\&At\ y=0,b:\ \ u_0=0,v_0=0,w_0=0,\ \varphi_x=0,\ \varphi_{y,y}=0\end{aligned} \tag{10b}$$

This set of partial differential equations should be numerically solved as a nonlinear eigenvalue problem in order to determine the frequency response of SLGSs carrying nanoparticles.

3. Numerical solution procedure

3.1. Pseudo-spectral solution procedure

Spectral methods are a class of numerical techniques in applied mathematics that have been widely applied to scientific problems [25]. The collocation version of the spectral method, called the pseudo-spectral (PS) method with the use of Chebyshev polynomials, can be profitable in the case of classical elasticity problems like beam, plates and shells analysis [26, 27]. The main idea in this method is to approximate the derivative of an unknown function, *F*, at a collocation point by an equivalent weighted linear sum of the function values at all collocation points. In one-dimensional domains, it is explained as follows:

$$\begin{aligned}&F_x^{(n)}(x_i)=\sum_{k=0}^{N}d_{ik}^{(n)}F(x_k)\ \ or\\&\left\{F_x^{(n)}\right\}_{(N+1)\times1}=\left[D^{(n)}\right]_{(N+1)\times(N+1)}\left\{F\right\}_{(N+1)\times1}\end{aligned} \tag{11}$$

where (N+1) is the number of collocation points, $F_x^{(n)}(x_i)$ indicates nth differentiation of function F in ith collocation point and [$D^{(n)}$] is called the nth differentiation matrix, the components of which the first derivative, [$D^{(1)}$] , based on Chebyshev basic functions, are [28]:

$$d_{00}^{(1)}=\frac{2N^2+1}{6},\ \ d_{NN}^{(1)}=-\frac{2N^2+1}{6} \tag{12a}$$

$$d_{jj}^{(1)}=\frac{-x_j}{2\left(1-x_j^2\right)},\ \ j=1,...,N-1 \tag{12b}$$

$$d_{ij}^{(1)} = \frac{c_i \left(-1\right)^{i+j}}{c_j \left(x_i - x_j\right)} \ , \ i \neq j \ \ , \ \ i,j = 0,...,N \qquad (12c)$$

$$c_i = \begin{cases} 2 & i = 0 or\ N\ ,otherwise \\ 1 & \end{cases} \qquad (12d)$$

The second differentiation matrix, $\left[D^{(2)}\right]$, can be easily computed as the square of $\left[D^{(1)}\right]$. Reference [28] provides some explicit formulas for higher-order differentiation matrices. The method can be extended to two-dimensional domains by explaining the *n*th partial derivative using Kronecker products as follows:

$$\left\{\frac{\partial^{(n)}F}{\partial x^{(n)}}\right\}_{(N+1)^2\times 1} = \left[D^{(n)} \otimes I\right]_{(N+1)^2\times(N+1)^2} \{F\}_{(N+1)^2\times 1} \qquad (13a)$$

$$\left\{\frac{\partial^{(m)}F}{\partial x^{(m)}}\right\}_{(N+1)^2\times 1} = \left[I \otimes D^{(m)}\right]_{(N+1)^2\times(N+1)^2} \{F\}_{(N+1)^2\times 1} \qquad (13b)$$

$$\left\{\frac{\partial^{(n+m)}F}{\partial x^{(n)}\partial y^{(m)}}\right\}_{(N+1)^2\times 1} = \left[D^{(n)} \otimes I\right]_{(N+1)^2\times(N+1)^2} \left[I \otimes D^{(m)}\right]_{(N+1)^2\times(N+1)^2} \{F\}_{(N+1)^2\times 1} \qquad (13c)$$

If ***A*** and ***B*** are two matrices of dimensions $p\times q$ and $r\times s$, respectively, then the Kronecker product, $\boldsymbol{A}\otimes\boldsymbol{B}$, is the matrix of dimension $pr\times qs$ with $p\times q$ block form, where the *i,j* block is *aij****B***. Additionally, ***I*** denotes the $(N+1)\times(N+1)$ identity matrix [28].

Chebyshev polynomials are orthogonal in the range of $[-1,1]$. Therefore, the rectangular real domain of nanoplate needs to be mapped to a 2×2 square computational domain using the following transformations.

$$\bar{x} = \frac{2x}{a} - 1 \ , \ \bar{y} = \frac{2y}{b} - 1 \ , \ \bar{x}, \bar{y} \in \left[-1,1\right] \qquad (14)$$

The grid points in both $\bar{x}$ and $\bar{y}$ directions are selected based on the Gauss-Lobatto interpolation points as follows in order to optimize the distribution [25]:

$$\bar{x}_i = cos\left(\frac{\pi i}{N}\right) , \ \bar{y}_i = cos\left(\frac{\pi i}{N}\right) , \ i,j = 0,1,2,...,N \qquad (15)$$

The following dimensionless parameters are introduced to render the problem dimensionless:

$$\begin{aligned} &\left(\bar{u}_0, \bar{v}_0, \bar{w}_0, \bar{z}_0, \bar{w}_{max}\right) = \left(u_0, v_0, w_0, z_0, w_{max}\right)/h \\ &\alpha = h/a \ , \ \beta = h/b \ , \ \gamma = a/b \\ &\bar{\mu} = \mu/a^2 \ , \ \bar{t} = \frac{t}{h}\sqrt{A/I_0}\left(\bar{\omega} = \Omega h\sqrt{I_0/A}\right) \\ &\bar{m} = M_0/phab \ \ , \ \ \bar{k} = K_0/A \end{aligned} \qquad (16)$$

where Ω and $\bar{\omega}$ are the factual and dimensionless natural frequencies of the system, respectively, and w_{max} is the maximum vibration amplitude. For the purpose of frequency analysis, the dimensionless displacement components are considered as:

$$\begin{Bmatrix} \bar{w}_0\left(\bar{x},\bar{y},\bar{t}\right) \\ \varphi_x\left(\bar{x},\bar{y},\bar{t}\right) \\ \varphi_y\left(\bar{x},\bar{y},\bar{t}\right) \\ \bar{u}_0\left(\bar{x},\bar{y},\bar{t}\right) \\ \bar{v}_0\left(\bar{x},\bar{y},\bar{t}\right) \\ \bar{z}_0\left(\bar{t}\right) \end{Bmatrix} = \begin{Bmatrix} \bar{w}_0\left(\bar{x},\bar{y}\right) \\ \varphi_x\left(\bar{x},\bar{y}\right) \\ \varphi_y\left(\bar{x},\bar{y}\right) \\ \bar{u}_0\left(\bar{x},\bar{y}\right) \\ \bar{v}_0\left(\bar{x},\bar{y}\right) \\ \bar{z}_0\left(\bar{t}\right) \end{Bmatrix} e^{i\,\bar{\omega}\bar{t}} \qquad (17)$$

Substituting Equation (14), (16) and (17) into Equation (9-10), the dimensionless nonlinear eigenvalue problem can be rewritten as follows:

$$\begin{aligned} &4\alpha^2\bar{u}_{,\bar{x}\bar{x}} + 8\alpha^3\bar{w}_{,\bar{x}}\bar{w}_{,\bar{x}\bar{x}} + \nu\left(4\alpha\beta\bar{v}_{,\bar{x}\bar{y}} + 8\alpha\beta^2\bar{w}_{,\bar{y}}\bar{w}_{,\bar{x}\bar{y}}\right) \\ &+ \frac{\left(1-\nu\right)}{2}\left(4\beta^2\bar{u}_{,\bar{y}\bar{y}} + 4\alpha\beta\bar{v}_{,\bar{x}\bar{y}} + 8\alpha\beta^2\left(\bar{w}_{,\bar{y}}\bar{w}_{,\bar{x}\bar{y}} + \bar{w}_{,\bar{x}}\bar{w}_{,\bar{y}\bar{y}}\right)\right) \\ &= -\bar{\omega}^2\left(\bar{u} - 4\bar{\mu}\bar{u}_{,\bar{x}\bar{x}} - 4\gamma^2\bar{\mu}\bar{u}_{,\bar{y}\bar{y}}\right) \end{aligned} \qquad (18a)$$

$$
\begin{aligned}
&4\beta^2\bar{v}_{,\bar{y}\bar{y}}+8\beta^3\bar{w}_{,\bar{y}}\bar{w}_{,\bar{y}\bar{y}}+\nu\left(4\alpha\beta\bar{u}_{,\bar{x}\bar{y}}+8\alpha^2\beta\bar{w}_{,\bar{x}}\bar{w}_{,\bar{x}\bar{y}}\right)\\
&+\frac{(1-\nu)}{2}\left(4\alpha^2\bar{v}_{,\bar{x}\bar{x}}+4\alpha\beta\bar{u}_{,\bar{x}\bar{y}}+8\alpha^2\beta\left(\bar{w}_{,\bar{x}}\bar{w}_{,\bar{x}\bar{y}}+\bar{w}_{,\bar{y}}\bar{w}_{,\bar{x}\bar{x}}\right)\right)\\
&=-\bar{\omega}^2\left(\bar{v}-4\bar{\mu}\bar{v}_{,\bar{x}\bar{x}}-4\gamma^2\bar{\mu}\bar{v}_{,\bar{y}\bar{y}}\right)
\end{aligned}
\tag{18b}
$$

$$
\begin{aligned}
&K_s\frac{(1-\nu)}{2}\left(4\alpha^2\bar{w}_{,\bar{x}\bar{x}}+4\beta^2\bar{w}_{,\bar{y}\bar{y}}+2\alpha\bar{\varphi}_{x,\bar{x}}+2\beta\bar{\varphi}_{y,\bar{y}}\right)\\
&+4\alpha^2\bar{w}_{,\bar{x}\bar{x}}\left[\left(2\alpha\bar{u}_{,\bar{x}}+2\alpha^2\bar{w}_{,x}^2\right)+\nu\left(2\beta\bar{v}_{,\bar{y}}+2\beta^2\bar{w}_{,\bar{y}}^2\right)\right]\\
&+4\beta^2\bar{w}_{,\bar{y}\bar{y}}\left[\left(2\beta\bar{v}_{,\bar{y}}+2\beta^2\bar{w}_{,\bar{y}}^2\right)+\nu\left(2\alpha\bar{u}_{,\bar{x}}+2\alpha^2\bar{w}_{,\bar{x}}^2\right)\right]\\
&+4(1-\nu)\alpha\beta\bar{w}_{,\bar{x}\bar{y}}\left(2\beta\bar{u}_{,\bar{y}}+2\alpha\bar{v}_{,\bar{x}}+4\alpha\beta\bar{w}_{,\bar{x}}\bar{w}_{,\bar{y}}\right)=-\bar{\omega}^2\left(\bar{w}-4\bar{\mu}\bar{w}_{,\bar{x}\bar{x}}-4\gamma^2\bar{\mu}\bar{w}_{,\bar{y}\bar{y}}\right)
\end{aligned}
\tag{18c}
$$

$$
\begin{aligned}
&4\alpha^2\bar{\varphi}_{x,\bar{x}\bar{x}}+4\nu\alpha\beta\bar{\varphi}_{y,\bar{x}\bar{y}}+2(1-\nu)\left(\beta^2\bar{\varphi}_{x,\bar{y}\bar{y}}+\alpha\beta\bar{\varphi}_{y,\bar{x}\bar{y}}\right)-6K_s(1-\nu)\left(\bar{\varphi}_x+2\alpha\bar{w}_{,\bar{x}}\right)\\
&=-\bar{\omega}^2\left(\bar{\varphi}_x-4\bar{\mu}\bar{\varphi}_{x,\bar{x}\bar{x}}-4\gamma^2\bar{\mu}\bar{\varphi}_{x,\bar{y}\bar{y}}\right)
\end{aligned}
\tag{18d}
$$

$$
\begin{aligned}
&4\beta^2\bar{\varphi}_{y,\bar{y}\bar{y}}+4\nu\alpha\beta\bar{\varphi}_{x,\bar{x}\bar{y}}+2(1-\nu)\left(\alpha^2\bar{\varphi}_{y,\bar{x}\bar{x}}+\alpha\beta\bar{\varphi}_{x,\bar{x}\bar{y}}\right)-6K_s(1-\nu)\left(\bar{\varphi}_y+2\alpha\bar{w}_{,\bar{y}}\right)\\
&=-\bar{\omega}^2\left(\bar{\varphi}_y-4\bar{\mu}\bar{\varphi}_{y,\bar{x}\bar{x}}-4\gamma^2\bar{\mu}\bar{\varphi}_{y,\bar{y}\bar{y}}\right)
\end{aligned}
\tag{18e}
$$

$$
\bar{k}\left[\bar{w}\left(\bar{x}_0,\bar{y}_0\right)-\bar{z}\right]=-\bar{\omega}^2\frac{\bar{m}}{\alpha\beta}\bar{z}
\tag{18f}
$$

The dimensionless integral governing equation is described as:

$$
\begin{aligned}
&\int_{-1}^{1}\int_{-1}^{1}\left\{K_s\frac{(1-\nu)}{2}\left(4\alpha^2\bar{w}_{,\bar{x}\bar{x}}+4\beta^2\bar{w}_{,\bar{y}\bar{y}}+2\alpha\bar{\varphi}_{x,\bar{x}}+2\beta\bar{\varphi}_{y,\bar{y}}\right)\right.\\
&+4\alpha^2\bar{w}_{,\bar{x}\bar{x}}\left[\left(2\alpha\bar{u}_{,\bar{x}}+2\alpha^2\bar{w}_{,x}^2\right)+\nu\left(2\beta\bar{v}_{,\bar{y}}+2\beta^2\bar{w}_{,\bar{y}}^2\right)\right]\\
&+4\beta^2\bar{w}_{,\bar{y}\bar{y}}\left[\left(2\beta\bar{v}_{,\bar{y}}+2\beta^2\bar{w}_{,\bar{y}}^2\right)+\nu\left(2\alpha\bar{u}_{,\bar{x}}+2\alpha^2\bar{w}_{,\bar{x}}^2\right)\right]\\
&+4(1-\nu)\alpha\beta\bar{w}_{,\bar{x}\bar{y}}\left(2\alpha\bar{u}_{,\bar{y}}+2\alpha\bar{v}_{,\bar{x}}+4\alpha\beta\bar{w}_{,\bar{x}}\bar{w}_{,\bar{y}}\right)\\
&\left.+\bar{\omega}^2\left(\bar{w}-4\bar{\mu}\bar{w}_{,\bar{x}\bar{x}}-4\gamma^2\bar{\mu}\bar{w}_{,\bar{y}\bar{y}}\right)\right\}d\bar{x}d\bar{y}=4\bar{k}\alpha\beta\left[\bar{w}\left(\bar{x}_0,\bar{y}_0\right)-\bar{z}\right]
\end{aligned}
\tag{18g}
$$

The dimensionless boundary conditions are:

Clamped (CCCC):

$$
At\ \bar{x}=-1,+1\ and\ \bar{y}=-1,+1:\quad \bar{u}=0,\bar{v}=0,\bar{w}=0,\bar{\varphi}_x=0,\bar{\varphi}_y=0
\tag{19a}
$$

SimplySupported (SSSS):

$$
\begin{aligned}
&At\ \bar{x}=-1,+1:\quad \bar{u}=0,\bar{v}=0,\bar{w}=0,\bar{\varphi}_y=0,\bar{\varphi}_{x,x}=0\\
&At\ \bar{y}=-1,+1:\quad \bar{u}=0,\bar{v}=0,\bar{w}=0,\bar{\varphi}_x=0,\bar{\varphi}_{y,y}=0
\end{aligned}
\tag{19b}
$$

One can obtain the discrete form of equations based on the pseudo-spectral method by applying Equation (13) to Equations (18a-f) and (19)

$$
\begin{aligned}
&4\alpha^2\left(D^{(2)}\otimes I\right)\{\bar{u}\}+8\alpha^3\left(D^{(1)}\otimes I\right)\{\bar{w}\}*\left(D^{(2)}\otimes I\right)\{\bar{w}\}\\
&+\nu\left(4\alpha\beta\left(D^{(1)}\otimes I\right)\left(I\otimes D^{(1)}\right)\{\bar{v}\}+8\alpha\beta^2\left(I\otimes D^{(1)}\right)\{\bar{w}\}*\left(D^{(1)}\otimes I\right)\left(I\otimes D^{(1)}\right)\{\bar{w}\}\right)\\
&+\frac{(1-\nu)}{2}\left(4\beta^2\left(I\otimes D^{(2)}\right)\{\bar{u}\}+4\alpha\beta\left(D^{(1)}\otimes I\right)\left(I\otimes D^{(1)}\right)\{\bar{v}\}\right.\\
&\left.+8\alpha\beta^2\left(\left(I\otimes D^{(1)}\right)\{\bar{w}\}*\left(D^{(1)}\otimes I\right)\left(I\otimes D^{(1)}\right)\{\bar{w}\}+\left(D^{(1)}\otimes I\right)\{\bar{w}\}*\left(I\otimes D^{(2)}\right)\{\bar{w}\}\right)\right.\\
&=-\bar{\omega}^2\left(\{\bar{u}\}-4\bar{\mu}\left(D^{(2)}\otimes I\right)\{\bar{u}\}-4\gamma^2\bar{\mu}\left(I\otimes D^{(2)}\right)\{\bar{u}\}\right)
\end{aligned}
\tag{20a}
$$

$$
\begin{aligned}
&4\beta^2\left(I\otimes D^{(2)}\right)\{\bar{v}\}+8\beta^3\left(I\otimes D^{(1)}\right)\{\bar{w}\}*\left(I\otimes D^{(2)}\right)\{\bar{w}\}\\
&+\nu\left(4\alpha\beta\left(D^{(1)}\otimes I\right)\left(I\otimes D^{(1)}\right)\{\bar{u}\}+8\alpha^2\beta\left(D^{(1)}\otimes I\right)\{\bar{w}\}*\left(D^{(1)}\otimes I\right)\left(I\otimes D^{(1)}\right)\{\bar{w}\}\right)\\
&+\frac{(1-\nu)}{2}\left(4\alpha^2\left(D^{(2)}\otimes I\right)\{\bar{v}\}+4\alpha\beta\left(D^{(1)}\otimes I\right)\left(I\otimes D^{(1)}\right)\{\bar{u}\}\right.\\
&\left.+8\alpha^2\beta\left(\left(D^{(1)}\otimes I\right)\{\bar{w}\}*\left(D^{(1)}\otimes I\right)\left(I\otimes D^{(1)}\right)\{\bar{w}\}+\left(I\otimes D^{(1)}\right)\{\bar{w}\}*\left(D^{(2)}\otimes I\right)\{\bar{w}\}\right)\right.\\
&=-\bar{\omega}^2\left(\{\bar{v}\}-4\bar{\mu}\left(D^{(2)}\otimes I\right)\{\bar{v}\}-4\gamma^2\bar{\mu}\left(I\otimes D^{(2)}\right)\{\bar{v}\}\right)
\end{aligned}
\tag{20b}
$$

$$
\begin{aligned}
&K_s\frac{(1-\nu)}{2}\left(4\alpha^2\left(D^{(2)}\otimes I\right)\{\bar{w}\}+4\beta^2\left(I\otimes D^{(2)}\right)\{\bar{w}\}+2\alpha\left(D^{(1)}\otimes I\right)\{\bar{\varphi}_x\}\right.\\
&+2\beta\left(I\otimes D^{(1)}\right)\{\bar{\varphi}_y\}+4\alpha^2\left(D^{(2)}\otimes I\right)\{\bar{w}\}\\
&*\left[\left(2\alpha\left(D^{(1)}\otimes I\right)\{\bar{u}\}+2\alpha^2\left(D^{(1)}\otimes I\right)\{\bar{w}\}*\left(D^{(1)}\otimes I\right)\{\bar{w}\}\right)\right.\\
&\left.+\nu\left(2\beta\left(I\otimes D^{(1)}\right)\{\bar{v}\}+2\beta^2\left(I\otimes D^{(1)}\right)\{\bar{w}\}*\left(I\otimes D^{(1)}\right)\{\bar{w}\}\right)\right]\\
&+4\beta^2\left(I\otimes D^{(2)}\right)\{\bar{w}\}*\left[\left(2\beta\left(I\otimes D^{(1)}\right)\{\bar{v}\}+2\beta^2\left(I\otimes D^{(1)}\right)\{\bar{w}\}*\left(I\otimes D^{(1)}\right)\{\bar{w}\}\right)\right.\\
&\left.+\nu\left(2\alpha\left(D^{(1)}\otimes I\right)\{\bar{u}\}+2\alpha^2\left(D^{(1)}\otimes I\right)\{\bar{w}\}*\left(D^{(1)}\otimes I\right)\{\bar{w}\}\right)\right]\\
&+4(1-\nu)\alpha\beta\left(D^{(1)}\otimes I\right)\left(I\otimes D^{(1)}\right)\{\bar{w}\}\\
&*\left(2\beta\left(I\otimes D^{(1)}\right)\{\bar{u}\}+2\alpha\left(D^{(1)}\otimes I\right)\{\bar{v}\}+4\alpha\beta\left(D^{(1)}\otimes I\right)\{\bar{w}\}*\left(I\otimes D^{(1)}\right)\{\bar{w}\}\right)\\
&=-\bar{\omega}^2\left(\{\bar{w}\}-4\bar{\mu}\left(D^{(2)}\otimes I\right)\{\bar{w}\}-4\gamma^2\bar{\mu}\left(I\otimes D^{(2)}\right)\{\bar{w}\}\right)
\end{aligned}
\tag{20c}
$$

$$
\begin{aligned}
&4\alpha^2\left(D^{(2)}\otimes I\right)\{\bar{\varphi}_x\}+4\nu\alpha\beta\left(D^{(1)}\otimes I\right)\left(I\otimes D^{(1)}\right)\{\bar{\varphi}_y\}\\
&+2(1-\nu)\left(\beta^2\left(I\otimes D^{(2)}\right)\{\bar{\varphi}_x\}+\alpha\beta\left(D^{(1)}\otimes I\right)\left(I\otimes D^{(1)}\right)\{\bar{\varphi}_y\}\right)\\
&-6K_s(1-\nu)\left(\{\bar{\varphi}_x\}+2\alpha\left(D^{(1)}\otimes I\right)\{\bar{w}\}\right)\\
&=-\bar{\omega}^2\left(\{\bar{\varphi}_x\}-4\bar{\mu}\left(D^{(2)}\otimes I\right)\{\bar{\varphi}_x\}-4\gamma^2\bar{\mu}\left(I\otimes D^{(2)}\right)\{\bar{\varphi}_x\}\right)
\end{aligned}
\tag{20d}
$$

$$
\begin{aligned}
&4\beta^2\left(I\otimes D^{(2)}\right)\{\bar{\varphi}_y\}+4\nu\alpha\beta\left(D^{(1)}\otimes I\right)\left(I\otimes D^{(1)}\right)\{\bar{\varphi}_x\}\\
&+2(1-\nu)\left(\alpha^2\left(D^{(2)}\otimes I\right)\{\bar{\varphi}_y\}+\alpha\beta\left(D^{(1)}\otimes I\right)\left(I\otimes D^{(1)}\right)\{\bar{\varphi}_x\}\right)\\
&-6K_s(1-\nu)\left(\{\bar{\varphi}_y\}+2\beta\left(I\otimes D^{(1)}\right)\{\bar{w}\}\right)\\
&=-\bar{\omega}^2\left(\{\bar{\varphi}_y\}-4\bar{\mu}\left(D^{(2)}\otimes I\right)\{\bar{\varphi}_y\}-4\gamma^2\bar{\mu}\left(I\otimes D^{(2)}\right)\{\bar{\varphi}_y\}\right)
\end{aligned}
\tag{20e}
$$

$$
\bar{k}\left[\bar{w}(\bar{x}_0,\bar{y}_0)-\bar{z}\right]=-\bar{\omega}^2\frac{\bar{m}}{\alpha\beta}\bar{z} \tag{20f}
$$

where$\{\bar{u}\}$, $\{\bar{v}\}$, $\{\bar{w}\}$, $\{\bar{\varphi}_x\}$ and $\{\bar{\varphi}_y\}$ are the vectors of dimension $(N+1)^2\times 1$, which indicate dimensionless displacement components in the grid points. The $(*)$ operator in nonlinear terms indicates component by component multiplying. In the case of simply supported boundary conditions, the spectral analogues of governing equations in the boundaries can be expressed as:

$$
\begin{aligned}
&At\ \bar{x}=-1,+1:\quad \left(D^{(1)}\otimes I\right)\{\bar{\varphi}_x\}=0\\
&At\ \bar{y}=-1,+1:\quad \left(I\otimes D^{(1)}\right)\{\bar{\varphi}_y\}=0
\end{aligned}
\tag{21}
$$

The standard matrix form of the eigenvalue problem of Equations (20) and (21) can be presented as follows:

$$
\left(\left[\tilde{K}\right]+\bar{\omega}^2[M]\right)\begin{Bmatrix}\{\bar{w}\}\\ \{\bar{\varphi}_x\}\\ \{\bar{\varphi}_y\}\\ \{\bar{u}\}\\ \{\bar{v}\}\\ \bar{z}\end{Bmatrix}=\{0\} \tag{22}
$$

It should be noted that Equation (20c) is valid in every grid point of the computational domain except the kth grid point, which is associated with the point (x_0, y_0) where the attached mass-spring system is located, due to the singularity of the lateral governing equation in this point. Therefore, the lateral governing equation needs to be replaced with the integral Equation (18g) in a way that will be explained in the following section.

3.2. Integral quadrature procedure

In the integral quadrature (IQ) method, the main idea is to evaluate the integration of an arbitrary function, H, on a domain by a weighted linear sum of the function values, H_i, at all grid points of the domain [29]. The IQ method for the present two-dimensional computational domain can be written as:

$$
\begin{aligned}
&\int_{-1}^{+1}\int_{-1}^{+1}H(\bar{x},\bar{y})d\bar{x}\,d\bar{y}=\sum_{i=1}^{(N+1)^2}L_iH_i\\
&=[L]_{1\times(N+1)^2}\{H\}_{(N+1)^2\times 1}
\end{aligned}
\tag{23}
$$

For applying the method, it is necessary to determine the associated weighting coefficients, l_i. This can be simply performed by introducing a set of $(N+1)^2$ polynomial test functions as follows [29]:

$$
H_t=X^mY^m\ ,\ m,n=0,\ldots,N \tag{24}
$$

As the values of these polynomials are known in the grid points and the values of their integrals on the domain can be easily computed, the weighting coefficients matrix, [L], will be evaluated through an inverse problem.

Here, the IQ method will be implemented to evaluate a discrete integral governing equation, Equation (18g), as follows:

$$
\begin{aligned}
&[L]\Big[K_s\frac{(1-\nu)}{2}\Big(4\alpha^2\Big(D^{(2)}\otimes I\Big)\{\bar{w}\}+4\beta^2\Big(I\otimes D^{(2)}\Big)\{\bar{w}\}+2\alpha\Big(D^{(1)}\otimes I\Big)\{\bar{\varphi}_x\}\\
&+2\beta\Big(I\otimes D^{(1)}\Big)\{\bar{\varphi}_y\}+4\alpha^2\Big(D^{(2)}\otimes I\Big)\{\bar{w}\}\\
&*\Big[\Big(2\alpha\Big(D^{(1)}\otimes I\Big)\{\bar{u}\}+2\alpha^2\Big(D^{(1)}\otimes I\Big)\{\bar{w}\}*\Big(D^{(1)}\otimes I\Big)\{\bar{w}\}\Big)\\
&+\nu\Big(2\beta\Big(I\otimes D^{(1)}\Big)\{\bar{v}\}+2\beta^2\Big(I\otimes D^{(1)}\Big)\{\bar{w}\}*\Big(I\otimes D^{(1)}\Big)\{\bar{w}\}\Big)\Big]\\
&+4\beta^2\Big(I\otimes D^{(2)}\Big)\{\bar{w}\}*\Big[\Big(2\beta\Big(I\otimes D^{(1)}\Big)\{\bar{v}\}+2\beta^2\Big(I\otimes D^{(1)}\Big)\{\bar{w}\}*\Big(I\otimes D^{(1)}\Big)\{\bar{w}\}\Big)\\
&+\nu\Big(2\alpha\Big(D^{(1)}\otimes I\Big)\{\bar{u}\}+2\alpha^2\Big(D^{(1)}\otimes I\Big)\{\bar{w}\}*\Big(D^{(1)}\otimes I\Big)\{\bar{w}\}\Big)\Big]\\
&+4(1-\nu)\alpha\beta\Big(D^{(1)}\otimes I\Big)\Big(I\otimes D^{(1)}\Big)\{\bar{w}\}\\
&*\Big(2\beta\Big(I\otimes D^{(1)}\Big)\{\bar{u}\}+2\alpha\Big(D^{(1)}\otimes I\Big)\{\bar{v}\}+4\alpha\beta\Big(D^{(1)}\otimes I\Big)\{\bar{w}\}*\Big(I\otimes D^{(1)}\Big)\{\bar{w}\}\Big)\\
&+\bar{\omega}^2\Big(\{\bar{w}\}-4\bar{\mu}\Big(D^{(2)}\otimes I\Big)\{\bar{w}\}-4\gamma^2\bar{\mu}\Big(I\otimes D^{(2)}\Big)\{\bar{w}\}\Big)\Big]\\
&=4\bar{k}\,\alpha\beta\big[\bar{w}(\bar{x}_0,\bar{y}_0)-\bar{z}\big]
\end{aligned}
\tag{25}
$$

Now, the singular lateral governing equation in *k*th grid point in Equation (22) is replaced with Equation (25) using the following matrix form:

$$
\big[\hat{I}\big]\left[\left(\big[\tilde{K}\big]+\bar{\omega}^2[M]\right)\begin{Bmatrix}\{\bar{w}\}\\ \{\bar{\varphi}_x\}\\ \{\bar{\varphi}_y\}\\ \{\bar{u}\}\\ \{\bar{v}\}\\ \bar{z}\end{Bmatrix}\right]=\big[\tilde{K}\big]\begin{Bmatrix}\{\bar{w}\}\\ \{\bar{\varphi}_x\}\\ \{\bar{\varphi}_y\}\\ \{\bar{u}\}\\ \{\bar{v}\}\\ \bar{z}\end{Bmatrix} \tag{26a}
$$

where

$$
\hat{I}_{ij}=\begin{cases}1 & i=j\ ,\ i\neq k\\ L_j & i=k\\ 0 & otherwise\end{cases} \tag{26b}
$$

Components of $[\hat{K}]$ are equal to zero, except for the two components in *k*th row, which contains terms from the right hand of Equation (25). Due to the simple form of matrices $[\hat{I}]$ and $[\hat{K}]$, Equation (26a) can be rewritten in the following form:

$$
\left(\big[\tilde{K}\big]+\bar{\omega}^2[M]\right)\begin{Bmatrix}\{\bar{w}\}\\ \{\bar{\varphi}_x\}\\ \{\bar{\varphi}_y\}\\ \{\bar{u}\}\\ \{\bar{v}\}\\ \bar{z}\end{Bmatrix}=0 \tag{27a}
$$

where

$$
\begin{aligned}
&[K]=\big[\tilde{K}\big]+\big[K^*\big]\\
&\big[K^*\big]=\big[\hat{I}\big]^{-1}\big[\hat{K}\big]=\big[\hat{K}\big]/l_k
\end{aligned}
\tag{27b}
$$

To establish the standard eigenvalue form of the problem, the displacement vectors can be divided to the boundary and the domain parts as follows:

$$
\begin{Bmatrix}\bar{w}_b\\ \bar{\varphi}_{xb}\\ \bar{\varphi}_{yb}\\ \bar{u}_b\\ \bar{v}_b\\ \bar{z}\end{Bmatrix}=\{b\}\ ,\ \begin{Bmatrix}\bar{w}_d\\ \bar{\varphi}_{xd}\\ \bar{\varphi}_{yd}\\ \bar{u}_d\\ \bar{v}_d\\ \bar{z}\end{Bmatrix}=\{d\} \tag{28}
$$

where subscripts *b* and *d* indicate boundary and domain, respectively. Then, the resulting eigenvalue of equations can be written in the matrix form as:

$$
\left(\begin{bmatrix}K_{bb} & K_{bd}\\ K_{db} & K_{dd}\end{bmatrix}+\bar{\omega}^2\begin{bmatrix}0 & 0\\ M_{db} & M_{dd}\end{bmatrix}\right)\begin{Bmatrix}b\\ d\end{Bmatrix}=0 \tag{29a}
$$

or

$$
\big[K_{bb}\big]\{b\}+\big[K_{bd}\big]\{d\}=0 \tag{29b}
$$

$$
\begin{aligned}
&\big[K_{db}\big]\{b\}+\big[K_{dd}\big]\{d\}=\\
&-\bar{\omega}^2\left(\big[M_{db}\big]\{b\}+\big[M_{dd}\big]\{d\}\right)
\end{aligned}
\tag{29c}
$$

Eliminating the boundary displacement vector,$\{b\}$, from Equation (29) one obtains,

$$
\left(\big[\bar{K}\big]+\bar{\omega}^2\big[\bar{M}\big]\right)\{d\}=0 \tag{30a}
$$

$$
\big[\bar{K}\big]=\big[K_{dd}\big]-\big[K_{db}\big]\big[K_{bb}\big]^{-1}\big[K_{bd}\big] \tag{30b}
$$

$$
\big[\bar{M}\big]=\big[M_{dd}\big]-\big[M_{db}\big]\big[M_{bb}\big]^{-1}\big[M_{bd}\big] \tag{30c}
$$

where $[\bar{M}]$ is the total mass matrix and $[\bar{K}]$ is the total stiffness matrix, which contains the linear and nonlinear stiffness terms and therefore is a function of displacements.

The nonlinear frequency response of SLGSs with an attached mass-spring system will be iteratively determined using the following stepwise algorithm: first, the nonlinear terms in stiffness matrix, $[\bar{K}]$, are neglected and the linear eigenvalue problem is solved in order to obtain the linear frequencies and associated mode shapes. Then, the mode shapes are scaled up to a given vibration amplitude, $\bar{w}_{max}$ and are used to calculate nonlinear coefficients. Following on, the updated eigenvalue problem is solved to determine the nonlinear frequencies and mode shapes. The iteration continues until the nonlinear eigenvalues converges with a desired accuracy [30].

4. Results and discussion

4.1. Validation study

The validation study is conducted to ensure the reliability and accuracy of the mathematic model and the pseudo-spectral nonlinear iterative procedure. In Table 1, the nonlinear to linear frequency ratio, $\bar{r}$, is presented for the case of the local continuum by setting the nonlocal small scale parameter equal to zero. The results agree very well with those of [31]. The influence of the small scale parameter on the linear frequency responses of nanoplates is indicated in Table 2. Excellent agreement with the exact results of a nonlocal FSDT plate model reported in [32] is observed, confirming the efficiency of the present method.

Table 1. Nonlinear frequency ratio, $\bar{r}$, of square SSSS plates. ($\boldsymbol{\nu = 0.3}$)

α	$\bar{w}_{max}$	Present	(Ref. [31])
0.001	0.2	1.0260	1.0250
	0.4	1.1011	1.1002
	0.6	1.2127	1.2080
	0.8	1.3567	1.3507
	1.0	1.5257	1.5134
0.1	0.2	1.0276	1.0266
	0.4	1.1071	1.1019
	0.6	1.2302	1.2194
	0.8	1.3781	1.3704
	1.0	1.5573	1.5413

Table 2. Dimensionless fundamental frequency $\bar{\omega}_{11} = \Omega h\sqrt{\rho/G}$ of SSSS square plate. ($\boldsymbol{a = 10\text{m},\ E = 30 \times 10^6\ \text{Pa},\ \nu = 0.3}$)

α	μ [m^2]	Present	Exact (Ref. [32])
0.05	0	0.0239	0.0239
	1	0.0218	0.0218
	2	0.0202	0.0202
	3	0.0189	0.0189
	4	0.0178	0.0178
	5	0.0169	0.0169
0.1	0	0.0930	0.0930
	1	0.0850	0.0850
	2	0.0788	0.0788
	3	0.0737	0.0737
	4	0.0695	0.0696
	5	0.0660	0.0660

4.2. Frequency shift and sensitivity of SLGS sensors

The capability of an SLGS as a resonant sensor is related to its frequency shift, Δf, due to changes in the value of attached mass, M_0. Frequency shift is defined as the difference between the fundamental frequency of an SLGS with attached nanoparticles, f, and the fundamental frequency of a bare SLGS, f_0; relative dimensionless frequency shift is indicated as $(\Delta f/f_0) = 1 - (f/f_0)$. The position of concentrated nanoparticles on the surface of SLGS is an important issue. Figure 2 gives the influence of the nanoparticle position on the linear dimensionless frequency shift of an SLGS, with $\bar{\mu} = 0.01$ carrying a nanoparticle of mass $\bar{m} = 0.5$. Although the absolute maximum frequency shift occurs when the nanoparticle is exactly located at the centre of SLGS, for a central area equal to 25% of the total sensing surface, the frequency shifts are at least 70% of the absolute maximum value. Frequency shifts decrease dramatically when approaching the boundaries of SLGS. From a practical point of view, it is difficult to place the nanoparticles exactly at the centre of SLGS. Nonetheless, the adsorbing mechanism should be optimized to locate nanoparticles as near as possible to the centre. The proposed combined numerical solution approaches has the ability to take into account the effect of position of attached nanoparticles on frequency shifts. All the results are nonetheless presented for nanoparticles located at the centre in order to show the maximum performance of the SLGS sensor.

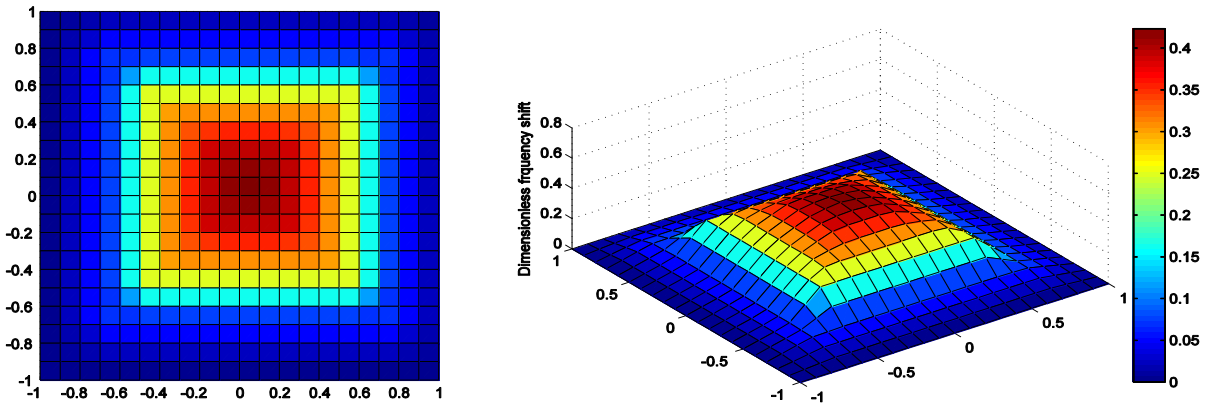

Fig. 2. Influence of nanoparticle position on dimensionless frequency shifts. Results are plotted on the dimensionless computational domain: $\bar{x}, \bar{y} \in [-1,1]$.

In order to investigate the influence of elastic connection between the SLGS and the attached mass, Figure 3 shows variation of linear $\Delta f / f_0$ versus variation of dimensionless spring constant, $\bar{k}$, for different values of thickness to side ratio, α. An attached mass of $\bar{m} = 0.5$ at the center of a simply supported square nanoplate with $\bar{\mu} = 0.01$ is considered. It is shown that for soft connections with small values of spring constant, the frequency shift reaches its maximum value, while increasing the rigidity of connection decreases the frequency shift to an ultimate frequency shift of a fully rigid connection. This means that considering a rigid connection instead of an elastic one will underestimate the frequency shift of nano resonant sensors. It should be noted that for very small spring constants, the connection between the nanoplate and the attached mass is not strong enough for allowing them to vibrate together, as they have a mode shape that corresponds to the first mode shape of a bare plate, but with a smaller frequency. Hence, the minimum value of $\bar{k} = 0.05$ is considered in presented results. Increasing thickness to side ratio decreases the dimensionless frequency of the nanoplate due to shear deformation effects [23]; however Figure 3 shows that increasing thickness to side ratio increases dimensionless frequency shift, especially for soft connections. For a nanoplate with a specified thickness, e.g., graphene sheets with h=0.34 nm, this means smaller sheets present a higher value of $\Delta f / f_0$ for a certain spring constant.

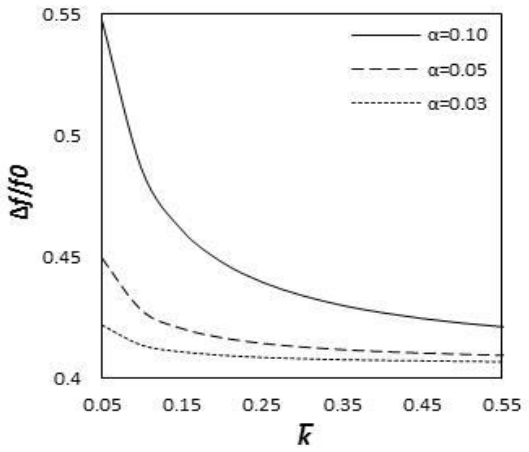

Fig. 3. Dimensionless linear frequency shift versus dimensionless spring constant for various values of thickness to side ratios

$\left(\bar{\mu} = 0.01, \bar{m} = 0.5, \gamma = 1, \bar{x}_0 = \bar{y}_0 = 0, B.C.: SSSS\right)$

Figure 4 illustrates dimensionless frequency shift versus dimensionless mass, attached at the centre of SLGS, for various values of vibration amplitude and nonlocal parameter. Results reveal that increasing $\bar{w}_{max}$ and decreasing $\bar{\mu}$ cause an increase in dimensionless frequency shift. To offer deeper insight into the relationship between these parameters, a general equation is proposed and is fitted to numerical results during a best fitting process as follows:

$$\frac{\Delta f}{f_0} = \left(1 + 0.13\bar{w}_{max}^2\right)\left(1 - \frac{1}{\sqrt{1 + \dfrac{4.4\bar{m}}{1 + 21\bar{\mu}}}}\right) \qquad (31)$$

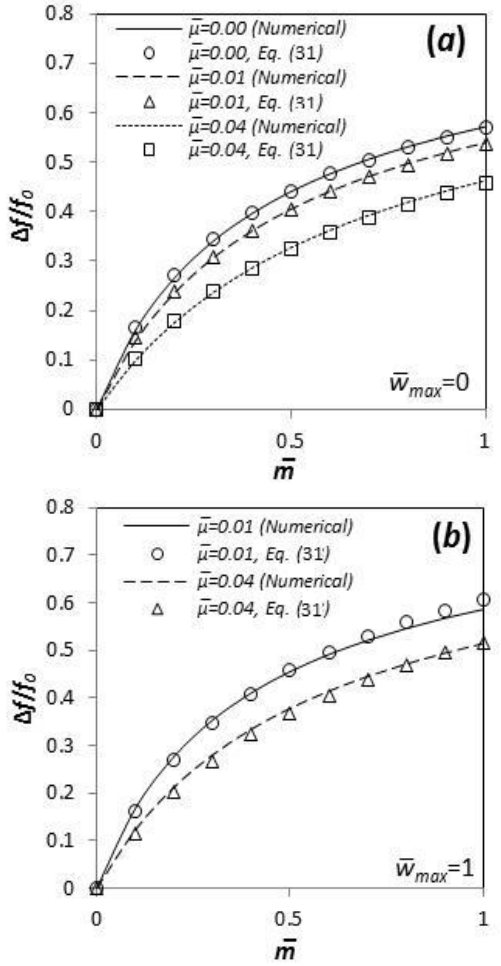

Fig. 4. Influence of (a) nonlocality and (b) nonlinearity on dimensionless frequency shift

The assumed general form of Equation (31) is taken from the equation presented in [11] for the linear dimensionless frequency shift of cantilever SLGS resonant sensors. Additionally, for adding nonlinear effects, an increasing factor is assumed, since the results show that nonlinearity increases dimensionless frequency shift proportional to the square of vibration amplitude, which shows the well-known hardening behaviour. Figure 4a compares numerical results with plots of Equation (31) for different values of nonlocal parameters (nonlinear effects are neglected). Figure 4b also presents nonlinear effects. It is seen that the plots of Equation (38) fit well with the obtained results.

Dimensionless sensitivity, *S*, is defined as the partial derivative of dimensionless frequency shift with respect to dimensionless mass, $\partial(\Delta f/f_0)/\partial(\bar{m})$. In the other words, sensitivity is equal to the slope of $(\Delta f/f_0)$-$\bar{m}$ curves and is therefore a function of dimensionless mass. It can be easily obtained from Equation (31) as:

$$S = \left(1+0.13\bar{w}_{max}^2\right)\left(\frac{2.2}{\left(1+21\bar{\mu}\right)\sqrt{\left(1+\frac{4.4\bar{m}}{1+21\bar{\mu}}\right)^3}}\right) \qquad (32)$$

Figure 5 demonstrates variations of dimensionless sensitivity versus dimensionless mass for various combinations of nonlinearity and nonlocality using Eqution (32). In general, sensitivity increases when the dimensionless mass decreases and the maximum sensitivity is achieved when the mass tends to zero; for values of dimensionless mass greater than one, $\bar{m} > 1$, sensitivity reduces dramatically and the effects of nonlinearity, nonlocality is almost ignored. This means SLGSs are not particularly sensitive to changes in the value of attached mass when they are detecting nanoparticles having the masses in the order of the mass of SLGS. One can observe that increasing the vibration amplitude and decreasing the nonlocal parameter increases the sensitivity of the SLGS resonant sensor.

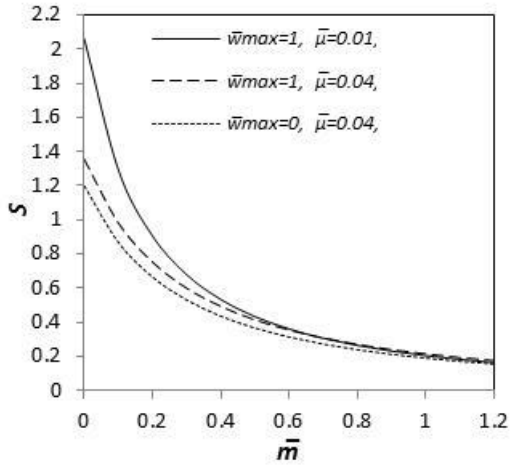

Fig. 5. Dimensionless sensitivity versus dimensionless mass with different combination of nonlinearity and nonlocality.

Boundary conditions can significantly affect the frequency shift. As it is expected, clamped boundaries present higher dimensionless frequency shift than simply supported ones due

to increasing total stiffness of the system. Table 3 lists the percent of enhancing of linear dimensionless frequency shift due to changing boundary conditions from simply supported to clamped boundaries. It is seen that when the dimensionless nonlocal parameter increases the enhancing effect of clamped boundaries increases. Also, SLGSs with clamped boundaries present greater enhancing effect when the dimensionless attached mass is smaller.

Table 3. Enhancing (%) of linear dimensionless frequency shift ($\Delta f/f_0$) due to changing boundary conditions from SSSS to CCCC

$\left(\alpha = 0.03, \gamma = 1, \bar{x}_0 = \bar{y}_0 = 0\right)$

		$\bar{\mu}$			
$\bar{m}$	$\bar{k}$	0.00	0.01	0.03	0.06
0.3	0.05	28.97	29.49	30.08	30.34
	0.25	23.98	24.14	24.27	24.39
0.5	0.05	22.12	22.92	24.21	25.53
	0.25	18.58	18.94	19.52	20.25
1.0	0.05	14.71	15.41	16.69	18.35
	0.25	12.60	12.97	13.64	14.55

5. Conclusion

In the present study, the potential application of single layered graphene sheets (SLGSs) as nano resonant mass sensors in detection of ultra-fine metallic nanoparticles is investigated based on nonlocal elasticity. A combination of pseudo-spectral and integral quadrature methods is implemented to numerically determine frequency shift and sensitivity of the sensor. The conclusions are listed as follows.

- Increasing vibration amplitude significantly increases the predicted frequency shift of SLGS resonant sensors.
- Increasing the small scale parameter causes a decrease in both frequency and frequency shift. This means that neglecting the nonlocal small scale parameter results in overestimating the frequency, frequency shift and sensitivity of the SLGS resonant sensor.
- Nanoplates with clamped boundary conditions present greater dimensionless frequency shift in comparison to simply supported ones, especially when the dimensionless attached mass is smaller.
- Decreasing the spring constant results in higher values of frequency shift. Therefore, it can be conclude that considering a rigid connection instead of elastic one will underestimate the frequency shift of nano resonant sensors.

References

[1].Mihindukulasuriya S.D.F., Lim L.T., 2014, Nanotechnology development in food packaging: A review, *Trends in Food Science & Technology* **40**(2): 149–167.

[2].Laroui H., Rakhya P., Xiao B., Viennois E., 2013, Merlin D., Nanotechnology in diagnostics and therapeutics for gastrointestinal disorders, *Digestive and Liver Disease* **45**(12) 995-1002.

[3].Eringen A.C., 2002, *Nonlocal Continuum Field Theories*, Springer-Verlag, New York.

[4].Danesh M., Farajpour A., Mohammadi M., 2012, Axial vibration analysis of a tapered nanorod based on nonlocal elasticity theory and differential quadrature method, *Mechanics Research Communications* **39**(1): 23-27.

[5].Mohammadi M., Ghayour M., Farajpour A., 2013, Free transverse vibration analysis of circular and annular graphene sheets with various boundary conditions using the nonlocal continuum plate model, *Composites Part B: Engineering* **45**(1): 32-42.

[6].Farajpour A., Rastgoo A., Mohammadi M., 2014, Surface effects on the mechanical characteristics of microtubule networks in living cells, *Mechanics Research Communications* **57**:18-26

[7].Wang Q., Wang C.M., 2007, The constitutive relation and small scale parameter of nonlocal continuum mechanics for modelling carbon nanotubes, *Nanotechnology,* doi:10.1088/0957-4484/18/7/075702.

[8].Wang Q., Arash B., 2014, A review on applications of carbon nanotubes and graphenes as nano-resonator sensors, *Comp. Mater. Sci.* **82**: 350–360.

[9].Shen Zh.B., Tang H.L., Li D.K., Tang G.J., 2012, Vibration of single-layered graphene sheet-based nanomechanical sensor via nonlocal Kirchhoff plate theory, *Comp. Mater. Sci.* **61**: 200–205.

[10]. Zhou Sh.M., Sheng L.P., Shen Zh.B., 2014, Transverse vibration of circular graphene sheet-based mass sensor via nonlocal Kirchhoff plate theory, *Comp. Mater. Sci.* **86**: 73–78.

[11]. Murmu T., Adhikari S., 2013, Nonlocal mass nanosensors based on vibrating monolayer graphene sheets, *Sensors Actuators B* **188**: 1319– 1327.

[12]. Adhikari S., Chowdhury R., 2012, Zeptogram sensing from gigahertz vibration: Graphene based nanosensor, *Physica E* **44**: 1528–1534.

[13]. Lee H.L., Yang Y.Ch., Chang W.J., 2013, Mass Detection Using a Graphene-Based Nanomechanical Resonator, *Jpn. J. Appl. Phys.* **52**: 025101.

[14]. Natsuki T., Shi J.X., Ni Q.Q., 2013, Vibration analysis of nanomechanical mass sensor using double-layered graphene sheets resonators, *J. Appl. Phys.* **114**, 094307.

[15]. Jomehzadeh E., Saidi A.R., Pugno N.M., 2012, Large amplitude vibration of a bilayer graphene embedded in a nonlinear polymer matrix, *Physica. E* **44**: 1973-1982.

[16]. Jomehzadeh E., Saidi A.R., 2011, A study on large amplitude vibration of multilayered graphene sheets, *Comp. Mater. Sci.* **50**: 1043-1051.

[17]. Shen L., Shen H.S., Zhang C.L., 2010, Nonlocal plate model for nonlinear vibration of single layer graphene sheets in thermal environments, *Comp. Mater. Sci.* **48**: 680-685.

[18]. Shen H.S., 2011, Nonlocal plate model for nonlinear analysis of thin films on elastic foundations in thermal environments. *Compos. Struct.* **93**: 1143-1152.

[19]. Jalali S.K. , Rastgoo A. , EshraghiI., 2011, Large amplitude vibration of imperfect shear deformable nano-plates using non-local theory, *Journal of Solid Mechanics* **3**(1): 64-73.

[20]. Malekzadeh P., Golbahar-Haghighi M.R., Shojaee M., 2014, Nonlinear free vibration of skew nanoplates with surface and small scale effects, *Thin.Wall. Struct.* **78**: 48–56.

[21]. Reddy J.N., 2008, *An Introduction to Continuum Mechanics*, Cambridge University Press, New York.

[22]. Eringen A.C., 1983, On differential equations of nonlocal elasticity and solutions of screw dislocation and surface waves, *J. Appl. Phys.* **54**: 4703.

[23]. Reddy J.N., 2003, *Mechanics of Laminated Composite Plates and Shells: Theory and Analysis*, CRC Press, New York, Second Edition.

[24]. Reddy J.N., 2010, Nonlocal nonlinear formulations for bending of classical and shear deformation theories of beams and plates, *Int. J. Eng. Sci.* **48**: 1507-1518.

[25]. Boyd J.P., 2000, *Chebyshev and Fourier Spectral Methods*, Dover, New York.

[26]. Jalali S.K., Naei M.H., Poorsolhjouy A., 2010, Thermal stability analysis of circular functionally graded sandwich plates of variable thickness using pseudo-spectral method. *Mater. Design*. **31**: 4755-4763.

[27]. Jalali S.K. , Naei M.H., Poorsolhjouy A., 2011, Buckling of circular sandwich plates of variable core thickness and FGM face sheets, *IJSSD* **11**(2): 273-295.

[28]. Trefethen L.N., 2000, *Spectral Methods in Matlab*. SIAM, Philadelphia.

[29]. Eftekhari S.A., Jafari A.A., 2012, Vibration of an initially stressed rectangular plate due to an accelerated traveling mass, *Scientia Iranica A* **19**(5): 1195–1213.

[30]. Malekzadeh P., 2008, Differential quadrature large amplitude free vibration analysis of laminated skew plates based on FSDT, *Compos. Struct.* **83**: 189-200.

[31]. Ganapathi M., Varadan T.K., Sarma B.S., 1991, Nonlinear flexural vibrations of laminated orthotropic plates, *Comput. Struct.* **39**(6): 685-688.

[32]. Aghababaei R., Reddy J.N., 2009, Nonlocal third-order shear deformation plate theory with application to bending and vibration of plates, *J. Sound. Vib.* **326**: 277-289.